AUTOMATIC FEATURE REGISTRATION AND DEM GENERATION FOR MARTIAN SURFACE MAPPING

F. XU [a,*], K. DI [a], R. LI [a], L.H. Matthies[b], and C.F. Olson [c]

[a]Department of Civil and Environmental Engineering and Geodetic Science, The Ohio State University
[b]Jet Propulsion Laboratory, California Institute of Technology
[c]University of Washington

Commission II, WG II/1

KEY WORDS: Mars Pathfinder, Imaginer for Mars Pathfinder (IMP), DEM, Panorama, Bundle adjustment, Registration, Interest points, Intra-stereo, Inter-stereo

ABSTRACT:

In this paper, we introduce the results of automatic registration, bundle adjustment, and DEM generation from panoramic close-range images taken on the 1997 Mars Pathfinder mission. Image registration is based on Förstner interest points, cross-correlation coefficient-based matching, parallax verification, and graph consistency verification. A free-network approach is used for bundle adjustment. The final product is a seamless DEM of the landing site created by a five-step process: automatic registration of intra-stereo images, coarse DEM generation, automatic registration of inter-stereo images, bundle adjustment of the entire panorama, and seamless DEM generation.

1. INTRODUCTION

Automation of surface mapping is important for Mars exploration. In the 1997 Mars Pathfinder mission, the landing vehicle (lander) along with the robot Sojourner returned thousands of images to Earth (Golombek et al., 1999). However, mapping of the landing site was not carried out in an automatic and near real-time way. Instructions for traversing and operations had to be sent from Earth to Mars each Martian night. Sojourner then followed those instructions the following day. Because rover localization errors accumulate, this mapping and navigation method has its limitation.

Future explorations of Mars will need to use an improved method because of the planned larger rover operation areas on the Martian surface. Upcoming missions include the 2003 Mars Exploration Rovers (MER) mission, the European Beagle 2 lander of the 2003 Mars Express mission, the 2007 Smart Lander and Long-range Rover mission, and sample return missions after 2010. During these missions, many panoramic images will be taken for mapping and rover localization purposes. If the rovers of these missions have automatic mapping abilities, they will be able to explore much farther on the Martian surface.

A DEM can be constructed from a set of panoramic images. Each section of DEM is generated by a pair of either intra- or inter-stereo images. Intra-stereo images are stereo panoramic images that are taken simultaneously by left and right cameras linked by a "hard" baseline. These images will have a large area of overlap. Images taken at different times and linked through "soft" baselines to form stereo images are called inter-stereo images. Inter-stereo images have only a small area of overlap (e.g., 10%). Due to errors in the initial orientation parameters, inconsistencies exist between images that can cause gaps between sections of DEM. To generate a seamless DEM (i.e. without any gaps or large elevation differences between the DEM sections), orientation parameters must be adjusted to suppress any inconsistencies (Kirk et al., 1999). A bundle-adjustment program has been developed to overcome these difficulties (Li et al., 2000, 2001; Ma et al., 2001; Di et al., 2002). To test the capability of mapping from panoramic images, we used images from Imaginer of the Mars Pathfinder (IMP). The image connection is not strong because the overlap between inter-stereo images is small (due to storage and transmission band limitations). However, panoramic images can overcome this difficulty by forming a closed image network.

Bundle adjustment requires tie points to connect the stereo images. The automation of tie point selection forms the main part of this paper.

2. METHODOLOGY

There are five steps in DEM generation: automatic registration of intra-stereo images, coarse DEM generation, automatic registration of inter-stereo images, bundle adjustment of the entire panorama, and seamless DEM generation.

2.1 Registration of Intra-Stereo Images

Registration of intra-stereo images consists of two stages: automatic matching of features and automatic verification of the matching result.

IMP cameras consist of a pair of stereo digital cameras with a 15-cm baseline, 14° FOV, and 0.023mm/pixel resolution. The overlap between intra-stereo images is over 90%.

Intra-stereo images within a pair are very similar except for coordinate differences (parallax) of same features that indicate depths from the cameras. The parallax can be calculated using image pointing information and is here simplified for understanding purpose:

$$p = b\frac{f}{d} \tag{1}$$

where p is the parallax
b is the baseline length
f is the focal length
d is the distance of the ground point from the camera

The maximum parallax (around 20 pixels for IMP images) of matched features can be estimated using the above equation.

2.1.1 Automatic Matching of Features

Points, lines or objects have been used in feature matching. To speed up the matching process of intra-stereo images, we chose interest points, which are simple yet very useful features including distinct point, end points of edges, and corners. Among various interest point operators (Sonka et al., 1999), we chose the Förstner operator (Förstner 1986) because it tends to provide more unique interest points in natural outdoor scenes. The Förstner operator is a filter that finds the local maximum of the following measure:

$$\frac{g_x^{\,2} g_y^{\,2} - g_{xy}^{\,2}}{g_x^{\,2} + g_y^{\,2}} \tag{2}$$

where g_x and g_y are the 1D gradients and g_{xy} is the 2D gradient of the grayscale image.

Our experiments indicate that the Förstner operator is very stable and that most interest points are identical for the same features under similar view-angles and illumination.

A typical IMP image can generate around 300~600 Förstner interest points (Figure 1), about the dimension of the image row. Therefore the matching of interest points over the entire image range has a computation complexity equal to that of epipolar line matching, which searches for matches along the epipolar line. If we add a constraint of maximum parallax, the search range for conjugate points can be further reduced to several points. Consequently, the matching of all interest points can be finished within a second on a P-III 500 computer.

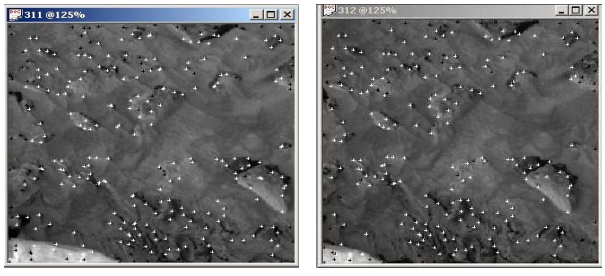

Figure 1. Interest points of intra-stereo images

The similarity between interest points is estimated by a cross-correlation coefficient. Once the coefficient between two interest points is larger than some threshold (e.g., 0.6) points are regarded as being matched. Typically, around 90% of interest points can find matches in this way. A typical matching result is shown in Figure 1 (white dots).

2.1.2 Automatic Verification of Matching Results

There exist mismatches. First, some interest points may exist in only one of the stereo images; thus, there are no correct matched points. This is particularly true in boundary areas outside of the overlap. The number of such mismatched points is proportional to the inter-stereo overlap, namely up to 10%. The second main cause of the mismatches can be attributed by non-unique features or repeated features. An image point may look similar to several possible points. This makes it difficult to select the correct match. This cause may account for only a relatively small amount of mismatches (normally less than 30%).

Mismatches can be suppressed by a spatial consistency constraint. Since the terrain is continuous, if two neighboring points in one image have matches in the other stereo image, the pair of conjugate points should have a spatial relationship. Any spatial disorder or inconsistency should indicate a mismatch.

Parallax consistency is one type of spatial consistency. If all matched points are ordered in the row direction from top to bottom and the parallax calculated as shown in Figure 2a where points are matched through the entire image range, we can see a general trend. Further constraints of epipolar geometry and the estimated elevation range can be employed eliminate some outliers. The rest of the parallaxes in the image can be combined to represent a smooth parallax curve with some variation. Small variations represent the continuous terrain changes and landmarks such as rocks (around 3~5 pixels). Large variations may represent peaks or valleys. The parallax curve represents spatial consistency

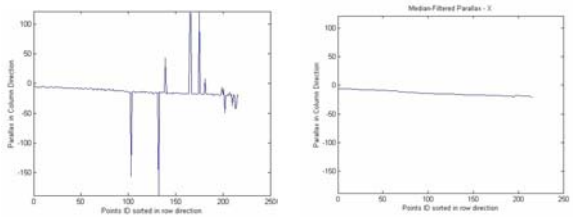

Figure 2. a) Parallax of matched interest points (left)
b) Extracted parallax curve (right)

Because the shape of the parallax curve is different for each image pair, we need to generate a curve and use it to suppress mismatches for each image pair individually. For intra-stereo stereo pairs, the overall mismatch ratio is low (less than 30%), and mismatches are evenly distributed along the parallax curve. Thus, we can use a median filter to filter out these mismatches and obtain the parallax curve as shown in Figure 2b.

A variation threshold is set up for the verification of matched points using the parallax curve. If the parallax of a matched pair relative to the parallax curve is less than the threshold, it will be regarded as a normal variation of the terrain; if greater, it will be treated as a mismatch and discarded.

As it is rare that two mismatched interest points are similar both in grayscale and spatial relationship, the parallax constraint can effectively eliminate most mismatches.

For the image in Figure 1a, 567 interest points were extracted; 387 (68%) of these were matched, of which 360 (93%) passed the parallax consistency verification test.

2.2 Coarse DEM Generation

Once the interest points from intra-stereo pairs are matched and verified, we can calculate the 3D ground coordinates by triangulations using the initial orientation parameters of the images. The initial orientation and position of IMP images were calculated from instrument elevation, azimuth and the lander surface quaternion provided in the image label data.

Before performing the bundle adjustment, we can generate a coarse DEM by interpolation and smoothing of the all 3D intra-stereo interest points. An example of this can be seen in Figure 3, where a total of 4,709 points from different intra-stereo pairs around the landing center are used to build a coarse DEM.

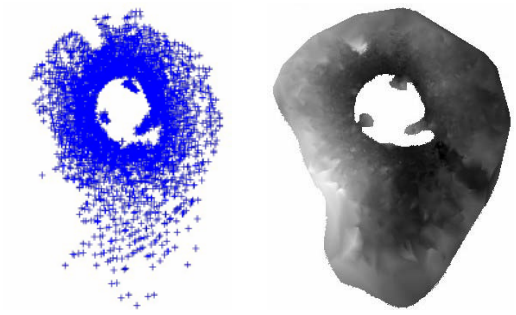

a. Distribution of interest points b. Coarse DEM

Figure 3. Coarse DEM generation

The coarse DEM provides a bridge for matching non-interest points, which can be valuable for use in DEM refinement. For a non-interest point, we can extend a line from the focal center through the image point until it hits the DEM and thereby obtain its 3D coordinates. We then project this point on to the adjacent stereo image to estimate the location of its conjugate point and search the conjugate points within a small range for a match. The coarse DEM also helps in matching interest points in an area between the inter-stereo images.

2.3 Automatic Registration of Inter-Stereo Images

A typical pair of inter-stereo images is shown in Figure 4. The amount of overlap (around 10%) can be estimated by projecting 3D interest points from one image onto the other to see whether they are located within a valid range of the image frame. The valid range is the maximum projection dislocation (around 20 pixels). The white dots in Figure 4 are interest points within the possible area of overlap.

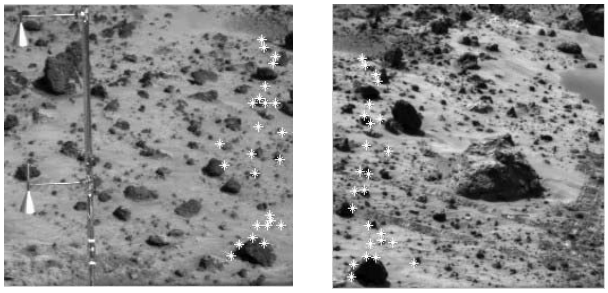

Figure 4. Interest points between inter-stereo images

Cross-correlation coefficients (CCC) were used in an attempt to match interest points within the possible area of overlap. The resulting percentage of mismatches was high, possibly due to a low threshold for the CCC. Furthermore, there may be some difference in illumination levels of the two inter-stereo images because the images were taken at different times. CCCs (around 0.6) between the same features, therefore, will not be as high as CCCs in intra-stereo images (around 0.9). To compensate, the threshold should be lower to extract additional possible matches. This will also increase the potential of mismatches. When trying to find a non-existing conjugate point, it may give a false conjugate point that appears to be similar enough (determined by the similarity threshold) to the original point. To get as many correct matches as possible, we apply the following strategy: first obtain as many matches as possible with a low CCC threshold, then verify these matches by checking their parallax consistency.

2.3.1 Automatic Matching of Inter-Stereo Interest Points

For each interest point, we project it from one image of a stereo pair to the other with the help of the coarse DEM. Its actual conjugate point should be within the maximum dislocation range of the projected position. For every pixel within this range, its CCC with the original point is calculated and compared to the coefficient threshold. From all points with coefficients larger than the threshold, the point with the maximum coefficient is selected as the conjugate point. Any mismatches are eliminated during the parallax consistency verification step that follows.

If more matches are needed, we can match non-interest points using the parallax curve. For each point in one image, we can predict the position of its conjugate point with the parallax curve, then search for the actual conjugate point within a small search range (determined by the terrain variation, 3~5 pixels). For such a small range, the mismatch ratio will be low even for non-interest points.

2.3.2 Parallax Consistency Verification

From Figure 5, we can see the difference between the parallax of inter-stereo and intra-stereo interest points. There are too many violations from the general trend of the parallax curve because of the high ratio of mismatches, which makes it difficult to derive a correct parallax curve directly from the original inter-stereo parallaxes.

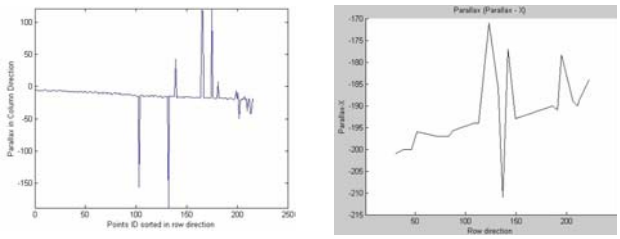

Figure 5. Parallax of matched intra-stereo (left) and inter-stereo (right) interest points

To extract the parallax curve, we need to use the coarse DEM generated in Step 2. Suppose the two inter-stereo images are horizontal. For these stereo images (see Figure 6), we can draw a vertical line in the middle of the overlapping region of the left image and select five evenly distributed points as white stars on the vertical line. We can then estimate their 3D coordinates using the coarse DEM and project them to the adjacent right

image. The parallaxes between the original positions in the left image and the projected positions in the right image are called predictive parallaxes (see Figure 7a).

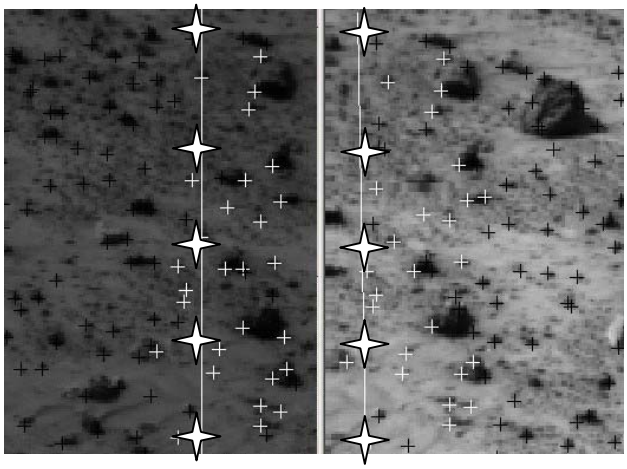

Figure 6. Parallax prediction. Stars are original positions (left image) and projected positions (right image)

As illustrated in Figure 7, the parallaxes (red dots) of the five points can be linked together and interpolated into a B-spline predictive parallax curve (blue lines) from which the inter-stereo parallaxes of all other image points can estimated.

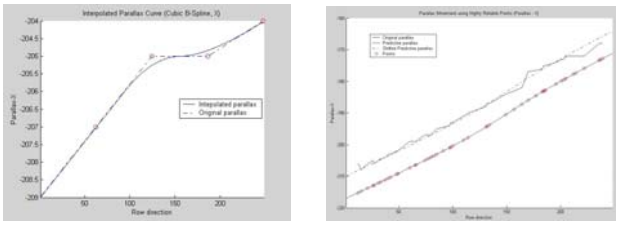

Figure 7a. Predictive parallaxes and predictive parallax curve (left); 7b. Movement of predictive parallax curve (right), where red dots are the location of parallaxes, solid curve is the interpolated parallax curve, and dotted curves are the actual parallax curves

The predictive parallax curve reflects terrain variations in the overlapping area, but it has shifted from the actual parallax curve due to imprecise azimuth and elevation angles. In Figure 7b, the predictive parallax curve is the solid blue curve, the actual parallax curve is the dotted blue curve, and the original parallax curve is the black solid line. The correct parallax curve can be obtained by shifting the predictive parallax curve. It should overlap with the original parallax. The shift can be estimated as follows.

For each pair of matched interest points, there are now two parallaxes: the actual parallax calculated by position difference between conjugate points and the predictive parallax calculated from the predictive parallax curve. The mean difference of these two gives an estimation of the movement between the predictive parallax curve and the actual parallax curve.

In calculating the movement of the parallax curve, we should not consider matched interest point pairs with low cross-correlation coefficients because they have a higher potential of mismatch. Only those pairs with high cross-correlation coefficients (>0.9) reliably provide correct matches and should be used. At this stage, the total number of matched interest point pairs is not a significant issue since just one pair of points will be enough to estimate the movement. Therefore we can use high cross-correlation ratio point pairs to estimate the parallax movement (Figure 8a), and then use the shifted parallax curve as the actual parallax curve to verify matched pairs with low cross-correlation ratios (Figure 8b). The original parallax of every point pair will be compared with its shifted predictive parallax. If the difference is within a valid range (mainly caused by terrain variation), this pair will be accepted as a correct match; otherwise, it will be treated as a mismatch and discarded.

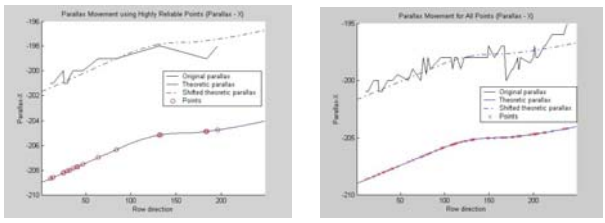

Figure 8a. Estimation of predictive parallax curve movement using matched point pairs with high cross-correlation coefficients (left); 8b. Original parallax, predictive parallax, and shifted parallax curves for all matched-point pairs

2.3.3 Link Graph Consistency Verification

All matched intra- and inter-stereo points are linked together to form a closed link graph. If there are mismatches, the graph will be broken into a tree, indicating an inconsistency.

There are two main types of link graph inconsistency: intra-stereo inconsistency and inter-stereo inconsistency. In intra-stereo inconsistency, intra-stereo interest points are registered with a high level of reliability and can be used to check inconsistency from inter-stereo matching. If a and b are one intra-stereo pair, and c and d are an adjacent intra-stereo pair, then there will be four combinations for matching: ac, ad, bc, and bd. Suppose a1 and b1 are conjugate points in a and b, and c1 and d1 are conjugate points in c and d. If a1 matches c1, then a1, b1, c1 and d1 should form a complete graph. In addition, a1 should also match d1, and b1 should match c1 and d1. Any exception to this will indicate inconsistency and will turn the graph into a tree by breaking linkages and introducing a new leaf. Any such matches should be discarded.

Figure 9. Result of link graph consistency verification

Tie points in inter-stereo overlapping areas passing the intra-stereo inconsistency check may still have inter-stereo inconsistency. If there are three inter-stereo pairs (a, b, and c)

with matched tie points (a1=b1, b1=c1), then a1, b1, c1 should form a complete graph. If a1 ≠ c1, however, then the graph is broken and inconsistency exists. All the matches are void and can't be used. Figure 9 is an example, where black dots are correct inter-stereo matches and white crosses are mismatches found by link graph consistency verification**.**

No automatic tie point consistency-checking method can guarantee zero mismatched points. It can only eliminate or suppress most mismatches so that they do not affect the subsequent bundle adjustment. Tie points passing all these checks are similar in grayscale neighborhood, and are consistent with correct parallaxes and with other tie points.

2.4 Bundle Adjustment of Entire Panorama

2.4.1 Panoramic Images

We used two panoramas created from 137 images, or around 68 pair. They are shown in Figure 10. They cover 360º of the azimuth. The tilt angle for the upper panorama ranged from 69~90º and the tilt angle for the lower panorama ranged from 50~69º. Overlapping exists in both the vertical and horizontal directions.

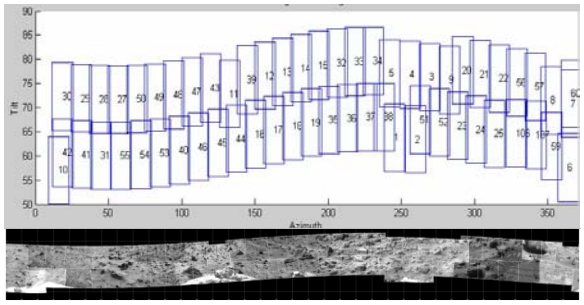

Figure 10. Structure of panoramic images (above: coverage of images; below: image mosaic provided by German DLR)

The precision of the relative orientation parameters among IMP images can be assessed using checkpoints in the overlapping area. Each feature point that exists in all four images of two adjacent intra-stereo pairs can serve as a checkpoint. From one intra-stereo pair, 3D coordinates can be derived and then projected to the adjacent stereo pair. The mean difference between projected and actual positions can then be used as an estimation of precision.

2.4.2 Bundle-Adjustment Model

Our bundle adjustment model is based on collinearity equations. The observation equation and its least-squares solution are represented in Equations (3) and (4):

$$AX = L \tag{3}$$

$$X = (A^T PA)^{-1}(A^T P)L \tag{4}$$

On the Martian surface there may not be a sufficient number control points, which are distinct landmarks such as remote mountain peaks that can be used to register surface images to orbital images. Therefore, the bundle adjustment used is a free network whose normal matrix is rank deficient. Thus no unique solution exists. We use the Singular Value Decomposition method to solve the normal equation in which a solution satisfies both the Least Squares principle and the Minimum Norm principle (Li et al., 2000, 2001; Ma et al., 2001; Di et al., 2002).

There are twelve unknown exterior orientation parameters for each pair of stereo images (X, Y, Z, azimuth, tilt, and swing). Only azimuth and tilt are independent in the lander coordinate system; the others are correlated. We represent the correlation between the exterior orientation parameters as a constraint expresses as Equation (5):

$$HX = W \tag{5}$$

Equations (3) and (5) can be combined in the form shown in Equation (6), in which the weights related to H should be set much higher than weights related to A.

$$\begin{bmatrix} V \\ W \end{bmatrix} = \begin{bmatrix} A \\ H \end{bmatrix} X - \begin{bmatrix} L \\ 0 \end{bmatrix} \tag{6}$$

Then the solution can be calculated in a manner similar to Equation (4).

2.4.3 Tie Point Selection

In bundle adjustment, we select nine tie points per intra-stereo pair and six points per inter-stereo pair (see Figure 11). These points are evenly distributed within the area of overlap.

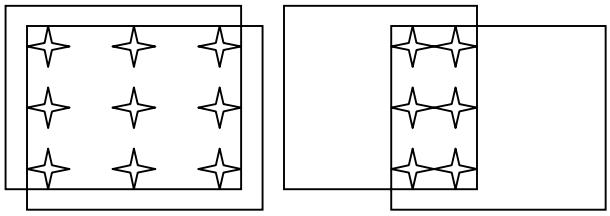

Figure 11. Distribution of tie points: a) intra-stereo images (left) and b) inter-stereo images (right)

It is important that tie points are evenly distributed. This is accomplished by drawing a grid (e.g. 3×3 grid) on the image and selecting one tie point that has the highest correlation coefficient in each patch.

It is also preferable that the same tie point appears in more images, i.e., it links more images. Thus, a point that exists in the greatest number of overlapping images is given the highest priority. This will further reduce redundancy and speed up calculation.

One example of distribution with sufficient control can be seen in Figure 11b. In the left-right inter-stereo pair, tie points should not be distributed in a single vertical column. Instead, they should be in at least two columns. For up-down inter-stereo distributions, tie points should be distributed in at least two rows.

In most stereo pairs, a sufficient number of tie points can be found within the 10% IMP overlap region. The link map of the entire panoramic images is shown in Figure 12. Strong links (more than four pair of evenly distributed tie points) are illustrated by solid lines and weak links (fewer than four pair) by dotted lines.

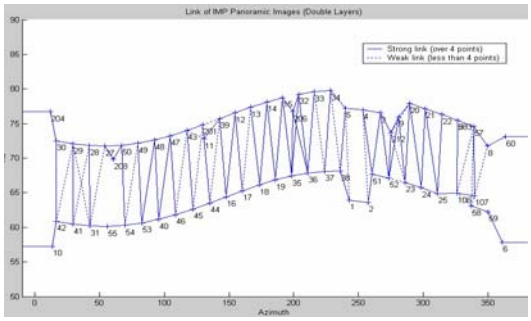

Figure 12. Link map of panoramic images

2.4.4 Bundle Adjustment

Bundle adjustment is used to improve the accuracy of the exterior orientation parameters and to provide high precision 3D ground points. Two comparisons were made among the configurations of the bundle adjustment. The first was a bundle adjustment of the entire panorama versus the partial panorama in order to check the importance of a closed panorama. The second was a bundle adjustment of upper panorama versus the lower panoramas in order to check the effectiveness of the horizontal link related to tilt angle. The results in both cases were compared to the original precision before bundle adjustment was made. The precision is depicted by projection dislocation, which is calculated by projecting interest points from one stereo pair to the adjacent pair and checking the difference between actual and projected positions.

The original precision results (before adjustment) were 11.5 / 44.1 / 1.11 as the mean/max/min error (in pixels) for the upper panorama and 9.3 / 43.2 / 0.54 as the mean/max/min error (in pixels) for the lower panorama.

As a result of the first comparison, the precision for the lower panorama is improved to 1.0 / 8.4 / 0.024 pixels as a loop and 1.3 / 9.3 / 0.0083 pixels without loop. For the upper panorama, results were 1.3 / 10.7 / 0.036 pixels as a loop and 2.6 / 52.7 / 0.0016 pixels as an open strip. We can see that a closed image loop improves the bundle adjustment.

In the second comparison, the bundle adjustment improved the precision to 1.0 / 8.4 / 0.024 pixels for the lower panorama and 1.3 / 10.7 / 0.036 pixels for the upper panorama. This indicates that lower tilt angles, larger overlapping, and stronger horizontal link contribute to higher mapping accuracy.

We are still working on the bundle adjustment of the combined panorama consisting of both upper and lower panoramas.

2.5 Seamless DEM Generation

The bundle adjustment provides improved exterior orientation parameters of the images as well as high precision 3D ground positions for all of the tie points. After the adjustment, more intra- and inter-stereo feature points can be matched with the help of the adjusted exterior orientation parameters. 3D ground positions of these points are calculated by triangulation. Then, all the 3D points are combined together to produce a seamless DEM by interpolation. Consequently, an orthoimage mosaic can be generated by projecting the DEM points back to the IMP image and assigning the corresponding gray value to the orthoimage. We are still working on the generation of the seamless DEM and orthoimage mosaic. We will present them at the symposium.

3. CONCLUSIONS

In this paper, we present the results of processing 1997 Mars Pathfinder IMP data. Our work focuses on automatic matching, verification, selection of intra- and inter-stereo tie points, bundle adjustment of panoramic images, and DEM generation. We successfully overcame challenges including low image overlap (around 10%), uneven depth distribution, and lack of absolute ground control. The techniques and software we have developed will be used to support the 2003 Mars Exploration Rovers mission.

ACKNOWLEDGEMENTS

We would like to acknowledge the help of Monika Hoyer, Marita Waehlisch and Dr. Jurgen Oberst of German DLR, and Dr. Ray Arvidson and Bethany Ehlmann of Washington University in St. Louis for providing data and valuable information on MPF IMP data processing. We would particularly like to thank Dr. Randy Kirk of USGS for his help on the conversion of IMP camera models. This research is being supported by JPL/NASA.

REFERENCES

DI, K., R. LI, F. XU, L.H. Matthies, C. Olson, 2002. High precision landing site mapping and rover localization by integrated bundle adjustment of MPF surface images. In: *ISPRS Commission IV 2002 Symposium*, Ottawa, Canada, July 8-12.

Golombek, M.P., et al., 1999. Overview of the Mars Pathfinder mission: Launch through landing, surface operations, data sets, and science results. *Journal of Geophysical Research*, 104(E4), pp. 8523-54.

Kirk, R.L., et al., 1999. Digital photogrammetric analysis of the IMP camera images: Mapping the Mars Pathfinder landing site in three dimensions. *Journal of Geophysical Research*, 104(E4), pp. 8869-88.

LI, R., F. MA, F. XU, L.H. Matthies, C. Olson and Y. Xiong, 2000. Large scale Mars mapping and rover localization using descent and rover imagery. In: *Proceedings of ISPRS 19th Congress*, Amsterdam, July 16-23 (CD-Rom).

LI, R., F. MA, F. XU, L.H. Matthies, C. Olson, and R.E. Arvidson, 2001. Localization of Mars rover using descent and surface-based image data. *Journal of Geophysical Research-Planet* (Accepted).

MA, F., K. DI, R. LI, L. Matthies, and C. Olson, 2001. Incremental Mars rover localization using descent and rover imagery. In: *ASPRS Annual Conference 2001*, St. Louis, MO, April 25-27 (CD-Rom).

Sonka, M., V. Hlavac, and R. Boyle, 1999. *Image Processing, Analysis, and Machine Vision*. Second Edition, J. Wiley & Sons, pp. 97.

XU, F., F. MA, R. LI, L. Matthies, and C. Olson, 2001. Automatic generation of a hierarchical DEM for Mars rover navigation. In: *Proceedings of the Third Mobile Mapping Conference*, Cairo, Egypt, January 3-5 (CD-Rom).